PAPER

Check for updates

Ca₃Lu(AlO)₃(BO₃)₄ : Sm³⁺: a novel red-emitting phosphor with high colour purity for NUV-based warm white LEDs†

Wasim ullah Khan,‡[a] Sunilkumar Baburao Mane, [ID] ‡[a] Salim ullah Khan,[b] Dongdong Zhou, [ID] [a] Dilfaraz Khan,[b] Qiaoxi Yu,[a] Weijie Zhou, [ID] [a] Lei Zhou,*[a] Jianxin Shi [ID] *[a] and Mingmei Wu [ID] *[a]

In the present work, we described the synthesis of a novel phosphor Ca₃Lu(AlO)₃(BO₃)₄ (CLAB) activated with Sm³⁺ via high temperature solid-state reaction. X-ray diffraction (XRD), FTIR spectra, diffuse reflection spectra, photoluminescence (PL) spectra and fluorescence decay curves were used to characterize the as-synthesized samples. The morphology and chemical composition were measured by field emission scanning electron microscope (FE-SEM) and X-ray energy diffraction spectroscopy (EDAX). The structure refinements from XRD data revealed the isostructural arrangement of CLAB : Sm³⁺ to gaudefroyite with a hexagonal P6₃/m space group in which the AlO₆ octahedral chains are interconnected by BO₃ triangles in the ab plane to form a Kagome-type lattice (star-shaped), leaving trigonal and apatite-like-tunnels. Under 404 nm excitation, the as-synthesized phosphor shows an intensely red emission peaked at 614 nm with CIE coordinates of (0.615, 0.380) and high colour purity up to 98.53%. The quantum yield of the phosphor was found to be 15.5% with a desired doping concentration of 5 mol% Sm³⁺ ions. The red emission intensity of CLAB : 0.05Sm³⁺ at 425 K is 86.6% of that at 300 K. All these good properties make the phosphor of CLAB : Sm³⁺ exhibit a great potential for application in UV-based warm white LEDs used in displays.

1. Introduction

White light-emitting diodes (LEDs) obtained from phosphors and LED chips have emerged as a promising next-generation light source to substitute conventional incandescent and fluorescent lamps owing to their significant energy efficiency, long operational lifetime, and environment friendliness.[1–4] In the present era, the extensively used approach to fabricate white LEDs is the combination of blue LED chips and a yellow-emitting phosphor, YAG : Ce³⁺. However, this approach suffers the drawback of low colour rendition (Ra < 80) due to the lack of red emission which hinders their extension to some applications.[5] In this regard, researchers have proposed an alternative method for fabricating white LEDs, by combining near ultraviolet (NUV) chips with green, blue and red tricolour phosphors.[6,7]

[a]MOE Key Laboratory of Bioinorganic and Synthetic Chemistry, School of Chemistry, Sun Yat-Sen University, Guangzhou 510275, P. R. China. E-mail: nx-zhoulei@foxmail.com; cessjx@mail.sysu.edu.cn; ceswmm@mail.sysu.edu.cn

[b]Institute of Chemical Sciences, Gomal University, Dera Ismail Khan, KPK, Pakistan

† Electronic supplementary information (ESI) available. See DOI: 10.1039/c8ra08374f

‡ Contributed equally and served as co-first authors.

Rong-Jun Xie and some researchers have reported that Y₂O₂S : Eu³⁺ and some nitrides or oxynitrides based compounds namely CaAlSiN₃ : Eu²⁺, M₂Si₅N₈ : Eu²⁺ (M = Ca, Sr and Ba) were used as red phosphors for NUV-based white LEDs.[8,9] However, Y₂O₂S : Eu³⁺ phosphor is not suitable due to its chemical instability and relatively low luminescence efficiency under excitation of NUV.[10] Furthermore, the nitrides and oxynitrides with good thermal stability have the disadvantages of being very expensive and having complex synthesis protocols including a high pressure of nitrogen and ultra-high temperature. Henceforth, it is a pressing requirement to achieve NUV-excitable oxide based red-emitting phosphors with high efficiency and good stability. Broadly speaking, rare earth ions have been playing an important role in preparing phosphors for lighting and display fields to generate multi-colour lights owing to the abundant emission colours based on their 4f → 4f or 5d → 4f transitions.[11–13]

The emission of Sm³⁺ is in the red spectral region which results from the transitions from excited ⁴G₅/₂ level to the ground state ⁶H₅/₂ and higher levels ⁶H$_J$ (J > 5/2). Sm³⁺ doped materials have been used as phosphors with narrow red-emitting and have shown promising applications in optical displays. Since the excitation band of Sm³⁺ is typically around 400 to 410 nm, which is better than that of Eu³⁺ at around 395 nm for NUV-emitting chip, consequently we have

employed Sm^{3+} ions to prepare red-emitting phosphors.[14,15] Furthermore, the selection of a suitable host material is very important to get high-efficiency inorganic phosphors. Borate has been proved to be an outstanding class of host materials for optical materials. Recently several groups reported the luminescence properties of rare earth ions doped Ca_3-$Y(AlO)_3(BO_3)_4$ phosphors.[16,17]

Henceforth, the present work described a novel red-emitting phosphor, $Ca_3Lu(AlO)_3(BO_3)_4 : Sm^{3+}$, with relatively high efficiency and high colour purity up to 98.53%. Upon the excitation of 404 nm, the phosphor displayed a strong red emission peak at 614 nm and the quantum yield was found to be 15.5% with a desired doping concentration of 5 mol% Sm^{3+} ion. All the results proved that the present synthesized phosphor is a suitable red-emitting applicant for optical displays and NUV-based white LEDs.

2. Experimental

2.1. Synthesis of $Ca_3Lu_{1-x}(AlO)_3(BO_3)_4 : xSm^{3+}$

A series of CLAB : xSm^{3+} (x = 0.01, 0.05, 0.10, 0.15, and 0.20) phosphors were synthesized using the conventional solid-state route. The reactants were as follows, Lu_2O_3 (A.R. grade), $CaCO_3$ (A.R. grade), H_3BO_3 (A.R. grade), $Al(OH)_3$ (A.R. grade), and Sm_2O_3 (99.99%). Materials in designed stoichiometric composition were thoroughly mixed and ground by pestle in an agate mortar. Subsequently, the well-ground mixture was transferred to an alumina crucible and calcined at 1100 °C for 4 h in air atmosphere. Finally obtained phosphors were ground again and forwarded for further measurements.

2.2. Measurements

X-ray diffraction (XRD) data of as-synthesized phosphors were collected using a Rigaku D-max 2200 diffractometer with Cu Kα radiation at 40 kV and 26 mA. XRD Rietveld profile refinements of the structural model were performed with the use of General Structure Analysis System (GSAS).[18,19] The crystal structures were drawn and analyzed with VESTA software.[20] The fourier transform infrared spectroscopy (FTIR) were investigated using a Shimadzu Spectrometer IRAffinity-1 model. The morphologies of the samples were characterized by a JEOL 840A field emission scanning electron microscope (FE-SEM) equipped with X-ray energy diffraction spectroscopy (EDAX). Diffuse reflection spectra (DRS) of the final synthesized phosphors were recorded at room temperature on a UV-visible-NIR spectrometer (Carry-5000). The photoluminescence excitation and emission spectra and fluorescence lifetime were collected with an FLS 920-combined Time-Resolved and Steady-State Fluorescence Spectrometer (Edinburgh) with photomultiplier tube operating at 400 V and Xe-lamp as an excitation source. And the temperature-dependent emission spectra were also collected on the same instrument with a temperature controller. The quantum yield of the synthesized phosphors was recorded on a Horiba FL3 (Japan) equipped with an integrating sphere.

3. Results and discussion

3.1. Crystal structure of $Ca_3Lu_{1-x}(AlO)_3(BO_3)_4 : xSm^{3+}$

After careful observation of the powder XRD pattern of prepared CLAB : xSm^{3+} (x = 0.01, 0.05, 0.15, and 0.20) phosphors as shown in Fig. 1(a), we can conclude that all the peaks resemble with those of standard $Ca_3Y(AlO)_3(BO_3)_4$ [Inorganic crystal structure database (ICSD-172154)].[21] Refinement of powder XRD profile for CLAB : $0.05Sm^{3+}$ shown in Fig. 1(b) was done by the General Structure Analysis System (GSAS). The crystallographic cell parameters of CLAB derived from the refined data are listed in ESI Table S1.†

The detailed crystal structural data after refinements for CLAB : $0.05Sm^{3+}$ phosphor were presented in Fig. 2(a and b) and ESI Table S1.† The crystal data confirm the $P6_3/m$ space group for CLAB : Sm^{3+} with AlO_6 octahedral share edges to form chains which are connected by triangular BO_3 groups in ab plane forming a Kagome-type lattice (star-shaped) along the c-axis similar to that in case of CYAB and the Lu(III) ion substitute
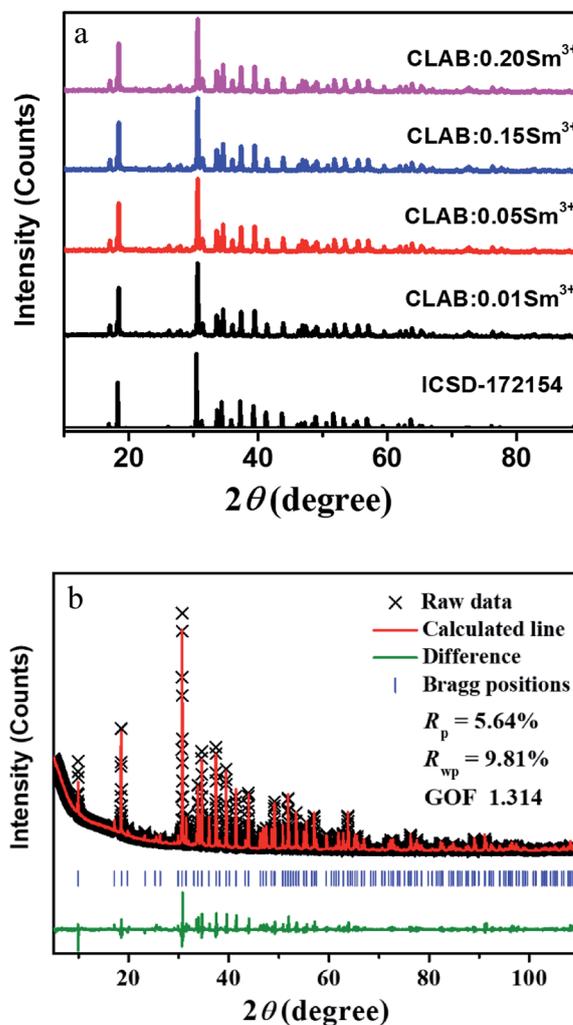

Fig. 1 XRD patterns (a) and Rietveld refinement results of CLAB : xSm^{3+} compared with the standard data of CYAB (ICSD-172154) (b).
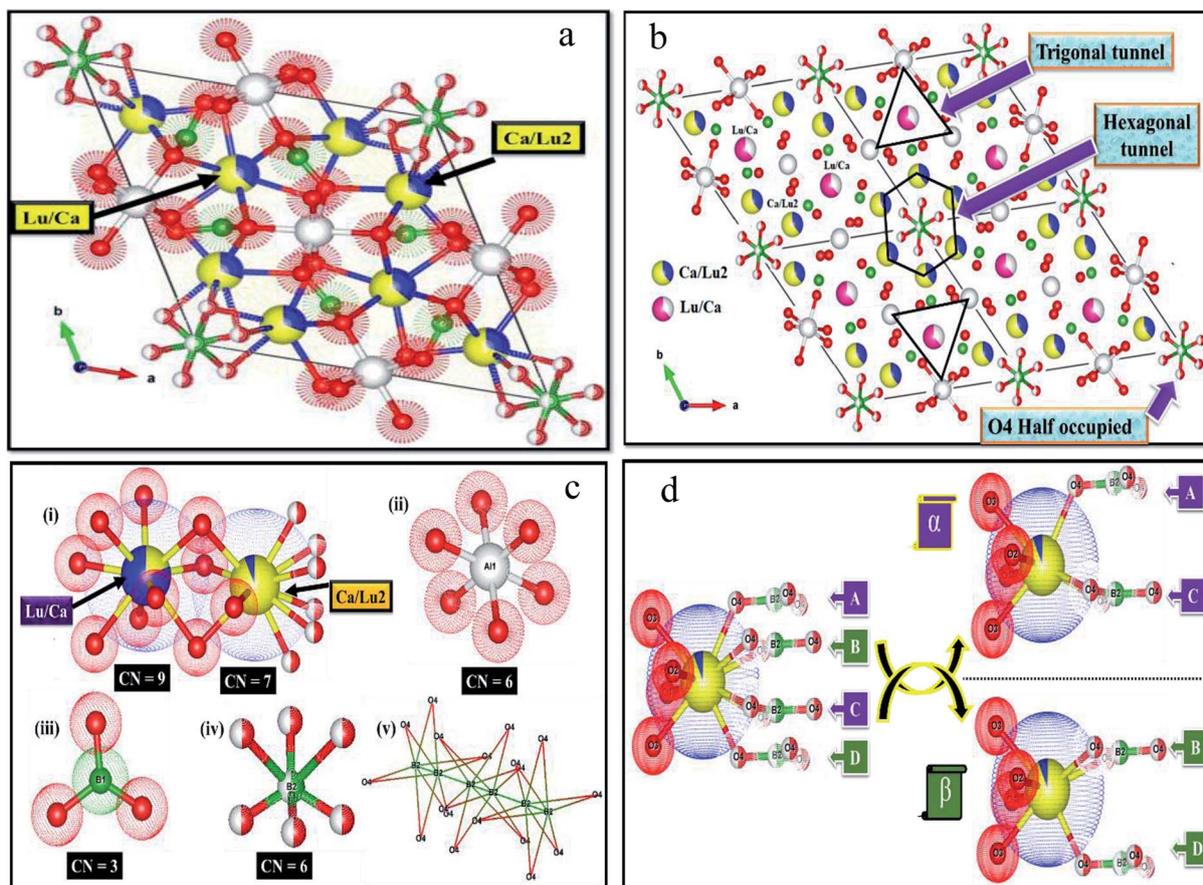
Fig. 2 Refined crystal structure of CLAB : Sm^{3+} (a), expanded view of (a) with $2 \times 2 \times 1$ cell (b), local environments at around all the atoms (i–v) (c), and conformation of the Lu/Ca site (d).

Y(III) to form the gaudefroyite lattice. The crystal structure comprises mainly two kinds of tunnels in the Kagome lattice, firstly a smaller trigonal tunnel which is occupied by the mixture of Lu/Ca ions and a larger apatite-like hexagonal tunnel which hosts Ca/Lu2 ions and isolated BO_3 groups. The metal ions in the Lu/Ca1 and Ca/Lu2 sites form 9 and 7-fold coordination structure after bonding with oxygen along with that the oxygen atom shared by Lu/Ca1 and Ca/Lu2 ions as displayed in Fig. 2(c).[21] The formation of $[BO_3]^{3-}$ triangle (A–D) is observed when the Ca/Lu2 sites are bounded by six half-occupied O4 ions shared by B(III) ions as shown in Fig. 2(d). Nevertheless, owing to the internal repulsion between the $[BO_3]^{3-}$ groups there are only two possible structural conformations are noticed for the Ca/Lu2 in their local environment for example, α and β sharing a chiral like relationship and subsequently the Ca/Lu2 sites composed of 7-fold coordinated structure rather than 10-coordination.[22] The characteristic metal oxygen configuration at the Lu/Ca1 site is clearly explained and the corresponding inter-atomic bond lengths of Lu/Ca1 to O and Ca/Lu2 to O in CLAB : $0.05Sm^{3+}$ are depicted in Table S2.† Three oxygen atoms categorized with O1 are situated in the same plane with a shorter bond length in the Lu/Ca1–O7 polyhedron as displayed in Fig. 2(c). The planer triangle coordination with the short bond length makes the Lu/Ca1 site compact even though Lu/Ca1 is 9-CN site. The Lu/Ca1 site prefers to occupy by smaller

cation owing to space hindering effect, which turns out to be the positive exclusion of larger Sm^{3+}.

There is much-pronounced tendency for Lu(III) ions to reside in the smaller trigonal tunnel and the relative ration of Lu/Ca in this tunnel is also correlated to the size of M(III) ion, with the highest Lu content (80%) for the smallest Al(III) ion. The trigonal tunnel is formed by Al–O–B–O six-membered ring whose size is determined by Al–O bond lengths. Smaller tunnels mean that the negative charge from the surrounding oxygen atoms is more concentrated, for the charge balance, ions with higher charge prefer to sit in, thus Lu(III) ion with a higher valence than Ca(II) tends to occupy the site in the trigonal tunnel.

3.2. FTIR and DRS of $Ca_3Lu_{1-x}(AlO)_3(BO_3)_4 : xSm^{3+}$

The FTIR spectra of undoped CLAB and Sm^{3+} doped (0.01, 0.05, 0.10, 0.15, and 0.20) samples recorded in the region 1600–400 cm^{-1} are displayed in Fig. 3(a). The strong broad peaks centred at 1330 cm^{-1} are assigned to asymmetric stretching vibrations of a B–O bond in the BO_3 group and the presence of Ca–O gives rise to a peak at 1217 cm^{-1}. Similarly, the weak peaks observed at 950 cm^{-1} and 920 cm^{-1} originate from the symmetric stretching vibrations of the B–O bond.[23,24] The peaks observed within the ranges of 760 to 721 cm^{-1} and 556 to 514 cm^{-1} are assigned to stretching and bending vibration of the Al–O and metal–oxygen either Al–O or Lu–O.[25,26] The broad

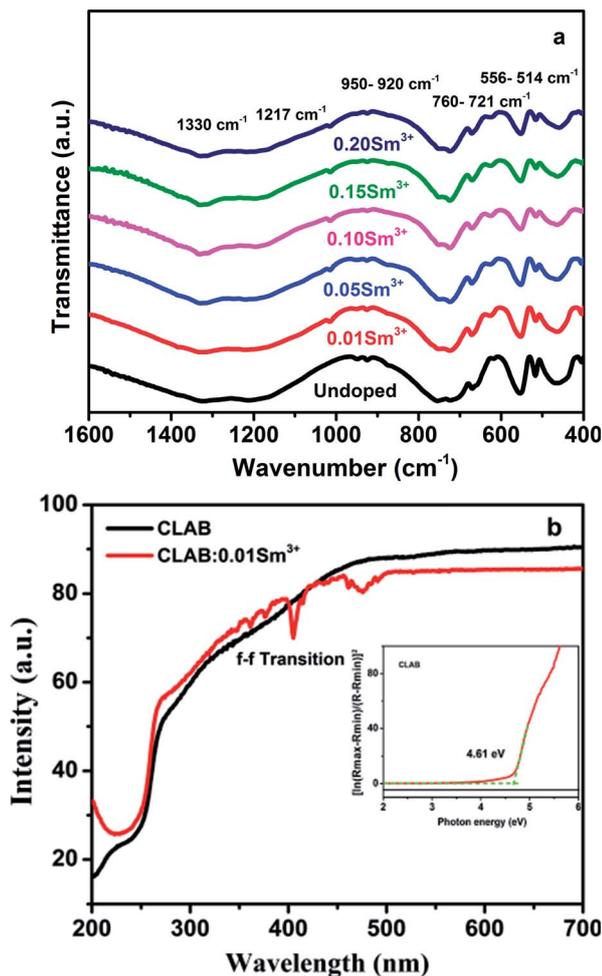**Fig. 3** FTIR spectra (a) and DRS of undoped CLAB and Sm^{3+} doped phosphor (b) [the inset shows the bandgap].

peak pointed at 466 cm^{-1} is the in-plane bending vibration of the B–O bond.[27] Hence, the above results provide the evidence for the formation of CLAB : xSm^{3+} phosphor.

CLAB host shows high light reflection in the range of 500–800 nm, and then it decreases in the range from 500 nm to 250 nm due to the light absorption by the host and keeps the same low level in the range from 250 nm to 200 nm as presented in Fig. 3(b). Results for CLAB : Sm^{3+} testify that the plateau of high reflectance is spread from longer wavelengths to 500 nm, and then it is declined slowly in the ultraviolet range at 200 nm. The bandgap of the host material is generally calculated by the following equation,[15]

$$\{\ln[(R_{max} - R_{min})/(R - R_{min})]\}^2 \ vs. \ h\nu \qquad (1)$$

where R is reflectance. The estimated value of E_g for the host is 4.61 eV.

3.3. Morphology of $Ca_3Lu_{1-x}(AlO)_3(BO_3)_4 : x$Sm^{3+}

The morphology of the prepared CLAB : xSm^{3+} phosphors has been elucidated by using FE-SEM. It is confirmed that the particles were closely packed with dimension in the micrometer

range including non-uniform particle size distribution with irregular structures as shown in Fig. 4(a and b). It was well documented that, closely packed particles display pronounced optical properties owing to low scattering of light, high packing density and bright luminescence, which produces efficient light output.[28] Besides, the EDAX of CLAB : xSm^{3+} phosphor (Fig. 4(c)) displays the presence of Ca, Lu, Al, B, O and Sm elements with homogenous distribution, which further provides the evidence that Sm^{3+} ions have been doped successfully into the CLAB host. The atomic and weight percentage distribution of elements are depicted in Table S3.†

3.4. PL properties of $Ca_3Lu_{1-x}(AlO)_3(BO_3)_4 : x$Sm^{3+}

The PLE spectrum of the red-emitting CLAB : Sm^{3+} phosphor is presented in Fig. 5(a). The excitation spectrum consists of series of narrow line peaks in the range from 200–500 nm, located at 344, 360, 374, 404, 422, 437, 460, and 475 nm. These peaks can be attributed to the f–f transitions of Sm^{3+} from $^6H_{5/2}$ to $^4H_{9/2}$, $^4D_{3/2}$, $^6P_{7/2}$, $^4F_{7/2}$, $^6P_{5/2}$, $^4G_{9/2}$, $^4I_{13/2}$, and $^4I_{11/2}$ levels, respectively. Amongst the representative 4f → 4f transition of Sm^{3+}, the strongest PLE peak at 404 nm is well matched with the emission wavelength of NUV LED chips.

The PL emission bands of CLAB : xSm^{3+} (x = 0.01, 0.05, 0.10, 0.15, and 0.20) phosphors consist of several orange-red emission peaks, which are attributed to $^4G_{5/2} \rightarrow {}^6H_{5/2}$ (564 nm), $^4G_{5/2} \rightarrow {}^6H_{7/2}$ (614 nm), $^4G_{5/2} \rightarrow {}^6H_{9/2}$ (647 nm), and $^4G_{5/2} \rightarrow {}^6H_{11/2}$ (708 nm) transitions from the excited level to the ground level of Sm^{3+}. The peak with the highest intensity was 614 nm originating from the typical $^4G_{5/2} \rightarrow {}^6H_{7/2}$ transition for Sm^{3+}.[29] It is found that the red emission intensity of $^4G_{5/2} \rightarrow {}^6H_{7/2}$ increases with the increase of Sm^{3+} concentration up to $x \sim 0.05$ where it reaches to the maximum. A further rise in Sm^{3+} concentration leads to a decrease in fluorescence owing to the concentration quenching. Additionally, the PL intensity of CLAB : xSm^{3+} decreases with the increases of Sm^{3+} concentration due to average distance among Sm^{3+} ions becomes shorter, resulting in more probable the energy transfer as shown in Fig. 5(b). Generally, exchange interaction, radiation absorption or multipole–multipole interaction may be responsible for non-radiative energy migration among Sm^{3+} ions. For the type of

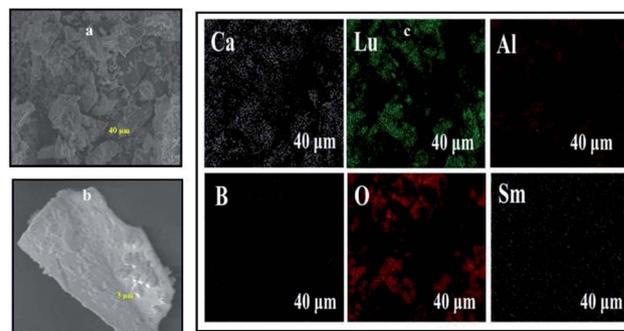**Fig. 4** Low-magnification (a), high-magnification FE-SEM image (b) and elemental X-ray dot mapping images (c) of CLAB : 0.05Sm^{3+} phosphor.

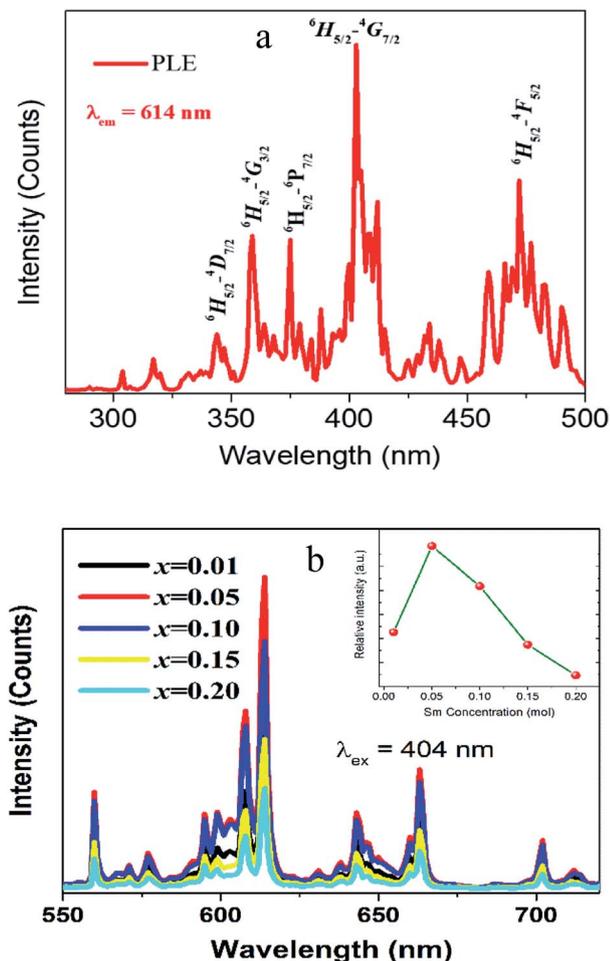**Fig. 5** PLE (a) and PL spectra (b) of CLAB : xSm^{3+} (x = 0.01, 0.05, 0.10, 0.15, and 0.20) [inset shows concentration dependent luminescence intensity].

the exchange interaction, there would be a tough requirement in the distance between the sensitizer and the activator (usually no more than 5 Å). The distance among ions can be estimated by using the equation,[30]

$$R \approx 2\left[\frac{3V}{4\pi x_c N}\right]^{1/3} \quad (2)$$

where N is the number of molecules in the unit cell, V is the cell volume and x_c is the total concentration of Sm^{3+}. For the CLAB host, $N = 2$, $V = 534.06$ Å^3 and the total concentration of activators are 0.05. Thus, the corresponding distance is calculated to be about 21.69 Å, indicating the little possibility of energy transfer *via* the exchange interaction. The process of radiation reabsorption takes effect only when the emission and absorption spectra are overlapped, which also does not take into effect in this case. Moreover, the resonant energy transfer mechanism for multipolar interactions can be further confirmed by using the following equation,[31]

$$\frac{I}{x} = \left[1 + \beta(x)^{Q/3}\right]^{-1} \quad (3)$$

where I is the emission intensity, x is the Sm^{3+} ions concentration, and β is a constant for the fixed host under the same excitation condition. Q can represent the multipolar interaction, whose values equal to 6, 8 and 10 corresponding to dipole–dipole, dipole–quadrupole or quadrupole–quadrupole, respectively. As represented in Fig. 6, the relationship between log(I/x) and log(x) can be fitted linearly, and the value of Q is determined to be 5.439 from the slope ($-Q/3 = -1.813$), which suggests that the concentration quenching mechanism in CLAB : xSm^{3+} phosphors is strongly accounted for by the dipole–dipole interaction.

The decay curves of CLAB : xSm^{3+} were obtained under the condition of monitoring at 614 nm with 404 nm excitation for different Sm^{3+} concentrations and are plotted in Fig. 7(a). It was found that all curves could be well fitted by the first-order exponential equation,[32]

$$I(t) = A\exp\left(-\frac{t}{\tau}\right) \quad (4)$$

where $I(t)$ is the luminescence intensity at time t, A is a constant and τ is the fluorescence lifetime, respectively. The fitted results for CLAB : 0.01Sm^{3+} are shown in Fig. 7(b). All the values of τ were calculated to be 1.89, 1.64, 1.37, 1.18, and 0.90 ms for CLAB : xSm^{3+} with x = 0.01, 0.05, 0.10, 0.15, and 0.20, respectively. The enhancement of non-radiative energy transfer among Sm^{3+} ions is responsible for the decreased lifetimes of CLAB : xSm^{3+} upon gradually increasing the concentration of Sm^{3+} ion.

To determine the energy transfer mechanism of Sm^{3+} ions in CLAB : xSm^{3+} phosphor, a simplified energy level diagram of Sm^{3+} ions along with the proposed luminescence processes is displayed in Fig. 8(a). In details, Sm^{3+} ions are first excited to the ^{4}H$_{9/2}$ level from the ground state of ^{6}H$_{5/2}$ when excited at 404 nm. After that, non-radiative (NR) transition takes place and the ^{4}G$_{5/2}$ level is populated, as shown in Fig. 8(a). Furthermore, the luminescence colour of CLAB : xSm^{3+} has been characterized using CIE 1931 chromaticity diagram.[33] The CIE coordinate value of the CLAB : 0.05Sm^{3+} phosphor is found to be (0.615,
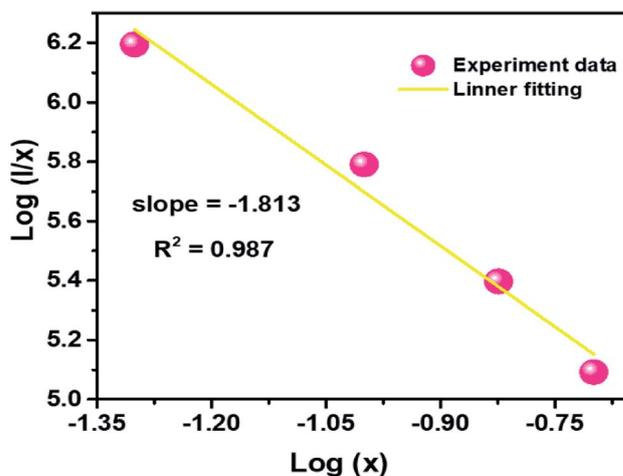

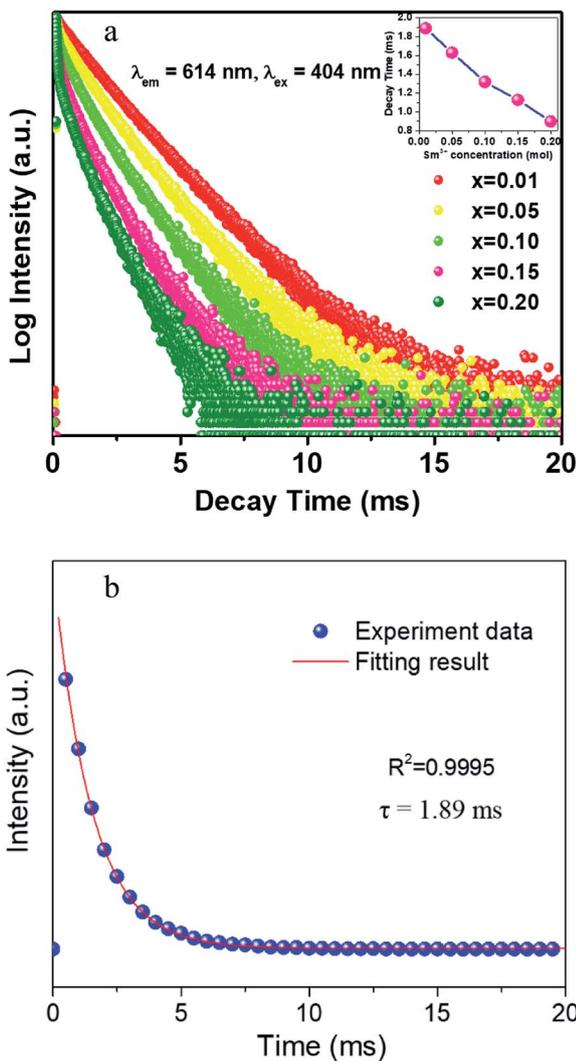**Fig. 6** Plot of log(I/x) versus log(x) for the 614 nm emission of Sm^{3+} ions in CLAB : xSm^{3+} phosphors.

Fig. 7 The decay curves of CLAB : xSm^{3+} (x = 0.01, 0.05, 0.10, 0.15, and 0.20) [inset, the related decay time in different concentration] (a) and the fitting results of CLAB : 0.01Sm^{3+} (b).
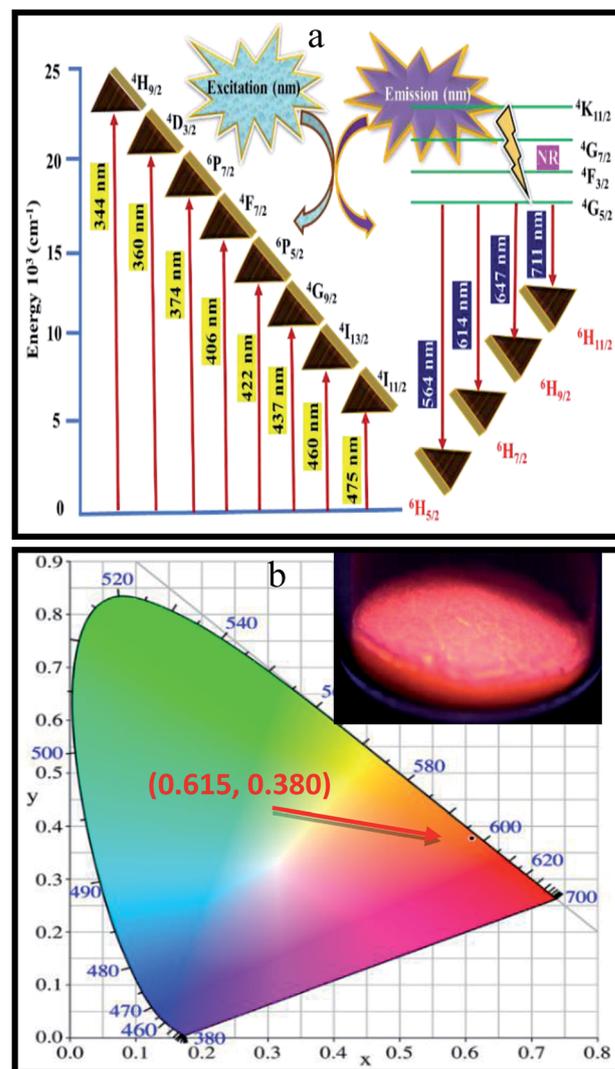

Fig. 8 Schematic energy level diagram showing the possible transitions of Sm^{3+} activator in the CLAB host (a) and CIE coordinates of CLAB : Sm^{3+} [inset, digital photograph of the phosphor under light of 365 nm] (b).

0.380), situated in the red region and at the extreme corner of the CIE diagram as shown in Fig. 8(b). Additionally, the colour purity is considered as one of the important factors for evaluating the performance of phosphors, the colour purity of the sample has been calculated by the following equation,[34,35]

$$\text{Colour purity} = \frac{\sqrt{(x - x_i) + (y - y_i)}}{\sqrt{(x_d - x_i) + (y_d - y_i)}} \times 100 \quad (5)$$

where (x, y) = (0.615, 0.380), CIE coordinates of CLAB : 0.05Sm^{3+} phosphor, (x_i, y_i) = (0.333, 0.333), CIE coordinates of white illumination and (x_d, y_d) = (0.6775, 0.3224), dominant wavelength (614 nm) of the phosphor respectively.[36] Consequently, the colour purity of the CLAB : 0.05Sm^{3+} was as high as 98.53% as shown in Table S4,† which seems to be better than the reported phosphors.[37] Apart from the above characteristics, the quantum yield is another vital parameter to identify the applicability of the resultant compounds for solid-state lighting. The quantum yield of the synthesized phosphors was

recorded on a Horiba FL3 (Japan) equipped with an integrating sphere. For CLAB : 0.05Sm^{3+} the excitation wavelength was set to be 404 nm.

And the emission ranging from 450 nm to 720 nm was recorded. The quantum yield (QY) of the CLAB : 0.05Sm^{3+} was determined to be 15.5% (see Fig. S1†). Compared with some reported phosphors, the QY of CLAB : 0.05Sm^{3+} seems to be much higher than those in the previous literatures.[37,38]

3.5. Thermal stability of Ca$_3$Lu$_{1-x}$(AlO)$_3$(BO$_3$)$_4$: 0.05Sm^{3+}

In general speaking, the phosphors play a key role in maintaining the emission intensities up to 425 K, because the temperature of the LED sources rises after used for a long time. The heat created by LED has a great influence on the colour rendering index and brightness output. The influence of temperature on the luminescence of CLAB : 0.05Sm^{3+} phosphor excited at 404 nm is presented in Fig. 9(a). As increasing

temperature from ambient temperature to 425 K the emission intensity of above-mentioned phosphor is only decreased 13.4%. Compared with some reported Sm^{3+} activated phosphors, such as $Y_2WO_6 : Sm^{3+}$, $Sr_3La(VO_4)_3 : Sm^{3+}$, $Ba_3La(PO_4)_3$- $: Tb^{3+},Sm^{3+}$, $CaSrSiO_4 : Ce^{3+},Sm^{3+}$ etc[15,37–39], the thermal stability of the as-synthesized phosphor seems to be much better. To further certify the relationship of luminescence with temperature and to determine the activation energy for thermal quenching, temperature-dependent PL spectra of CLAB : $0.05Sm^{3+}$ were fitted by using Arrhenius formula,[40,41]

$$\frac{I}{I_0} = \left[1 + C \exp\left(-\frac{\Delta E}{kT}\right)\right]^{-1} \tag{6}$$

in which I_0 is the initial emission intensity at room temperature, whereas I is the intensity at different testing temperature T, C is a constant for a certain host, k is Boltzmann constant and ΔE is the activation energy for thermal quenching. Through a best fitting curve using Arrhenius formula, ΔE was calculated to be 0.232 eV for Sm^{3+} in CLAB : $0.05Sm^{3+}$ phosphor as shown in Fig. 9(b).

To evaluate the practical feasibility of the CLAB : $0.05Sm^{3+}$ for solid-state lighting, a red-emitting LED device was prepared by integrating an InGaN NUV chip (∼380 nm) and the CLAB : $0.05Sm^{3+}$ phosphor. Under the forward bias current of 100 mA, the electroluminescent spectrum of the fabricated red-emitting LED device was recorded as shown in Fig. S2.† Clearly, the EL spectrum was composed of several emission bands. The emission peak situated at approximately 380 nm is assigned to the center wavelength of the chip, while the other peaks come from the transitions of Sm^{3+} activators, respectively. Moreover, the prepared LED device can emit brightly red light that can be seen by the naked eyes (see Fig. S2†), revealing that the Sm^{3+}-activated CLAB is a promising red-emitting phosphor for display and white LEDs.

4. Conclusion

In conclusion, we described the synthesis of the new phosphor of $Ca_3Lu(AlO)_3(BO_3)_4 : Sm^{3+}$ which shows an intense red emission with high colour purity up to 98.53%. The structure refinements from X-ray powder diffraction revealed the isostructural arrangement of CLAB : Sm^{3+} to gaudefroyite with a hexagonal $P6_3/m$ space group to form a Kagome-type lattice (star-shaped), leaving trigonal and apatite-like-tunnels. The red emission intensity of CLAB : $0.05Sm^{3+}$ at 425 K is 86.6% of that at 300 K, showing a good thermal stability and a potential application for NUV-based white LEDs used in displays.

Conflicts of interest

There are no conflicts to declare.

Acknowledgements

References

1 Z. Wang, F. Yuan, X. Li, Y. Li, H. Zhong, L. Fan and S. Yang, *Adv. Mater.*, 2017, **29**, 1702910.
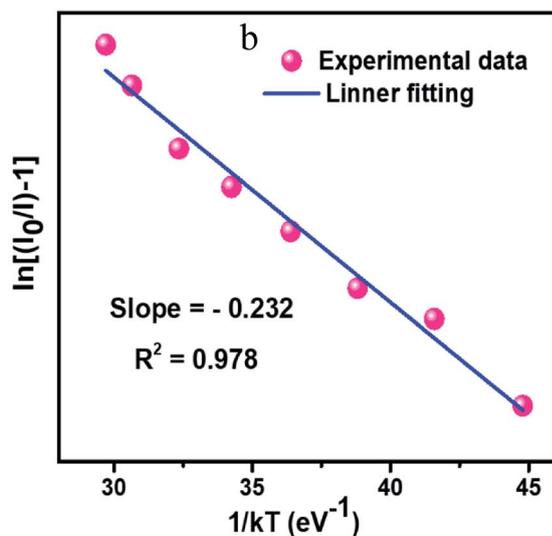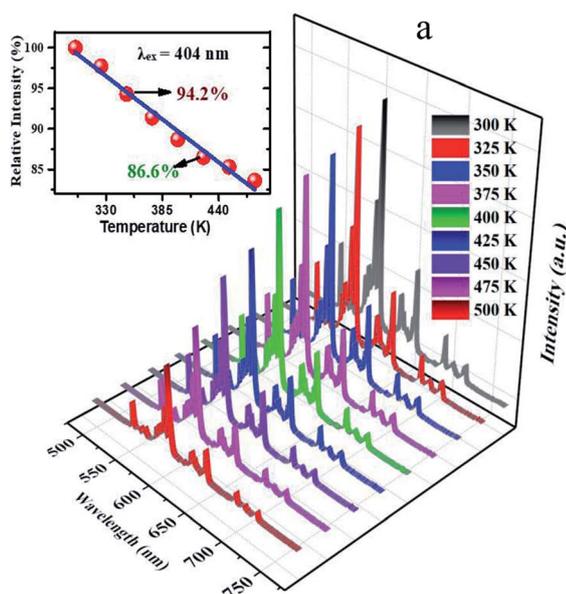

Fig. 9 Temperature-dependent photoluminescence spectra ranging from 300 K to 500 K and related integrated intensities in different temperature (a) and Arrhenius fitting results of CLAB : $0.05Sm^{3+}$ (b).

2 J. Li, Q. Liang, J.-Y. Hong, J. Yan, L. Dolgov, Y. Meng, Y. Xu, J. Shi and M. Wu, *ACS Appl. Mater. Interfaces*, 2018, **10**, 18066–18072.

3 W. Dai, Y. Lei, J. Zhou, Y. Zhao, Y. Zheng, M. Xu, S. Wang and F. Shen, *J. Am. Chem. Soc.*, 2017, **100**, 5174–5185.

4 J. Li, J. Yan, D. Wen, W. U. Khan, J. Shi, M. Wu, Q. Su and P. A. Tanner, *J. Mater. Chem. C*, 2016, **4**, 8611–8623.

5 J. Li, Z. Zhang, X. Li, Y. Xu, Y. Ai, J. Yan, J. Shi and M. Wu, *J. Mater. Chem. C*, 2017, **5**, 6294–6299.

6 Q. Zhang, X. Wang, X. Ding and Y. Wang, *Inorg. Chem.*, 2017, **56**, 6990–6998.

7 P. Du, X. Huang and J. S. Yu, *Chem. Eng. J.*, 2018, **337**, 91–100.

8 R.-J. Xie, N. Hirosaki, Y. Li and T. Takeda, *Materials*, 2010, **3**, 3777–3793.

9 P. Pust, V. Weiler, C. Hecht, A. Tücks, A. S. Wochnik, A.-K. Henß, D. Wiechert, C. Scheu, P. J. Schmidt and W. Schnick, *Nat. Mater.*, 2014, **13**, 891.

10 Y. Huang, Y. Nakai, T. Tsuboi and H. J. Seo, *Opt. Express*, 2011, **19**, 6303–6311.

11 G. Blasse and B. Grabmaier, in *Luminescent Mater.* Springer, 1994, pp. 91–107.

12 X. Huang, B. Li, H. Guo and D. Chen, *Dyes Pigm.*, 2017, **143**, 86–94.

13 C.-H. Huang and T.-M. Chen, *J. Phys. Chem. C*, 2011, **115**, 2349–2355.

14 Z.-W. Zhang, Y.-S. Peng, X.-H. Shen, J.-O. Zhang, S.-T. Song and Q. Lian, *J. Mater. Sci.*, 2014, **49**, 2534–2541.

15 W. Khan, L. Zhou, Q. Liang, X. Li, J. Yan, N. ur Rahman, L. Dolgov, S. U. Khan, J. Shi and M. Wu, *J. Mater. Chem. C*, 2018, **6**, 7612–7618.

16 W. U. Khan, J. Li, X. Li, Q. Wu, J. Yan, Y. Xu, F. Xie, J. Shi and M. Wu, *Dalton Trans.*, 2017, **46**, 1885–1891.

17 S. Wang, Q. Sun, B. Li, H. Guo and X. Huang, *Dyes Pigm.*, 2018, **157**, 314–320.

18 A. C. Jensen, M. Hinge and H. Birkedal, *CrystEngComm*, 2015, **17**, 6940–6946.

19 B. H. Toby, *J. Appl. Crystallogr.*, 2001, **34**, 210–213.

20 K. Momma and F. Izumi, *J. Appl. Crystallogr.*, 2011, **44**, 1272–1276.

21 Y. Yu, Q. Wu and R. Li, *J. Solid State Chem.*, 2006, **179**, 429–432.

22 D. Wen, H. Kato, M. Kobayashi, S. Yamamoto, M. Mitsuishi and M. Kakihana, *J. Mater. Chem. C*, 2017, **5**, 4578–4583.

23 S. Rada, M. Culea, M. Rada, P. Pascuta, V. Maties and E. Culea, *J. Mol. Struct.*, 2009, **937**, 70–74.

24 K. Feng, W. Yin, J. Yao and Y. Wu, *J. Solid State Chem.*, 2011, **184**, 3353–3356.

25 R. Schroeder and L. Lyons, *J. Inorg. Nucl. Chem.*, 1966, **28**, 1155–1163.

26 A. Garcıa-Murillo, C. Le Luyer, C. Pedrini and J. Mugnier, *J. Alloys Compd.*, 2001, **323**, 74–77.

27 L. Jun, X. Shuping and G. Shiyang, *Spectrochim. Acta, Part A*, 1995, **51**, 519–532.

28 J. Wan, L. Cheng, J. Sun, H. Zhong, X. Li, W. Lu, Y. Tian, H. Lin and B. Chen, *J. Alloys Compd.*, 2010, **496**, 331–334.

29 R. Shi, J. Xu, G. Liu, X. Zhang, W. Zhou, F. Pan, Y. Huang, Y. Tao and H. Liang, *J. Phys. Chem. C*, 2016, **120**, 4529–4537.

30 D. Wen, J. Feng, J. Li, J. Shi, M. Wu and Q. Su, *J. Mater. Chem. C*, 2015, **3**, 2107–2114.

31 X. Huang, S. Wang, B. Li, Q. Sun and H. Guo, *Opt. Lett.*, 2018, **43**, 1307–1310.

32 W. U. Khan, D. Wang, W. Zhang, Z. Tang, X. Ma, X. Ding, S. Du and Y. Wang, *Sci. Rep.*, 2017, **7**, 14866.

33 R. Hunt, *Color Res. Appl.*, 1991, **16**, 146–165.

34 Z. Lou and J. Hao, *Thin Solid Films*, 2004, **450**, 334–340.

35 J. S. Kumar, K. Pavani, A. M. Babu, N. K. Giri, S. Rai and L. R. Moorthy, *J. Lumin.*, 2010, **130**, 1916–1923.

36 R. A. Kumar, S. Hata, K.-I. Ikeda and K. Gopchandran, *RSC Adv.*, 2016, **6**, 67295–67307.

37 P. Du and J. S. Yu, *J. Lumin.*, 2017, **32**, 1504–1510.

38 A. M. Kaczmarek, K. Van Hecke and R. Van Deun, *Inorg. Chem.*, 2014, **53**, 9498–9508.

39 W. Zhou, M. Gu, Y. Ou, C. Zhang, X. Zhang, L. Zhou and H. Liang, *Inorg. Chem.*, 2017, **56**, 7433–7442.

40 L. Zhou, H. Liang, P. A. Tanner, S. Zhang, D. Hou, C. Liu, Y. Tao, Y. Huang and L. Li, *J. Mater. Chem. C*, 2013, **1**, 7155–7165.

41 X. Huang, B. Li and H. Guo, *J. Alloys Compd.*, 2017, **695**, 2773–2780.